Novel Electrically Controlled Rapidly Wavelength Selective Photodetection Using MSMs

Ray Chen, *Student Member, IEEE*, David A. B. Miller, *Fellow, IEEE*, Kai Ma, *Student Member, IEEE*, and James S. Harris, Jr., *Fellow, IEEE*

***Abstract*—A novel electrically controlled tunable metal–semiconductor–metal (MSM) photodetector is introduced and experimentally demonstrated with 2.5-ns wavelength-switching access time on a GaAs chip for switching between two wavelengths. This detector has a demonstrated 20.1-dB ON/OFF contrast ratio between the selected and the rejected wavelength and can resolve 179-GHz spaced wavelength-division multiplexing channels. In addition, device wavelength switching is achieved with a differential input voltage swing of ± 1.65 V. This low bias voltage makes it compatible with complementary metal-oxide semiconductor (CMOS) control electronics for rapid switching.**

***Index Terms*—Access network, dense wavelength division multiplexing (DWDM), metal–semiconductor–metal (MSM) photodetector, optical code division multiple access (OCDMA), reconfigurable wavelength-division multiplexing (WDM) network, telecommunication, tunable filter, tunable photodetector.**

I. Introduction

RAPID wavelength tuning is potentially useful in modern packet-switching optical networks [1]. Dynamic wavelength allocation in optical networks allows efficient bandwidth usage in the presence of bursty Internet traffic [2]. Currently, tunable transmitters rather than tunable receivers are more widely considered in network designs because of the transmitters' much shorter tuning times. Rapidly tunable photodetectors (receivers) would also allow rapid wavelength reallocation and could provide further flexibility in network designs. Conventional tunable photodetectors/filters are usually tuned acoustically, mechanically, or thermally. Unfortunately, their wavelength-switching access time ranges are relatively slow, ranging from a few seconds to a few microseconds, depending on the device's working principle [3]–[6]. Tunable photodetectors based on electroabsorption and electrorefraction tuning mechanisms have the potential to tune rapidly, but often they have small tuning and working range and may require large bias voltage that may prevent their integration with complementary metal-oxide semiconductor (CMOS) electronics [7]. Active tunable filters tuned by current injection might also tune rapidly, but they have severe difficulties in wavelength stabilization and suffer from mode-hopping problems [8]. Cascaded Mach-Zehnder interferometers have also been designed as rapidly tunable wavelength filters and they have been demonstrated to switch between wavelengths with 50-ns access time [9], but the tuning range is only a few nanometers and the insertion loss is high.

In this paper, we propose a novel electrically controlled metal–semiconductor–metal (MSM) tunable photodetector which could potentially switch wavelengths as rapidly as the switching time of the electronic controller. This device has multiple detector fingers and is operated under the illumination of an optical beam interfering with a delayed version of itself. The relative phase between the resulting interference fringes and the device fingers is a function of the wavelength, and the wavelength resolution of this tunable detector is set by the amount of delay between the beams. When the wavelength is tuned, the interference pattern moves across the device and the relative phase between the interference pattern and the device changes. Since the polarity of photocurrent of a MSM device depends on the electrode biasing polarity, we can design the polarity of the MSM electrode biasing pattern digitally to reject certain interference patterns while responding to others, thus determining the spectral response of the photodetector. In addition, the low biasing voltages needed means this device could also be integrated with CMOS electronics for rapid control of the spectral sensitivity to achieve an integrated system on a chip. In this paper, we demonstrate device wavelength switching with only ± 1.65-V biasing. In addition, this has a wide potential tuning range. This controllable biasing goes beyond previous proposals for fixed multifinger wavelength detection [10].

II. Device Operation Principle

The key to the operation of this device is the interference of a beam with a delayed version of itself on a multifingered detector. Fig. 1, which shows the apparatus used in our experiments, is one example way to do this. Many other methods to set up such a wavelength dependent interference pattern are possible [10]. The apparatus in Fig. 1 generates a wavelength dependent interference pattern that lines up with the device fingers. Adjusting the mirror positions also adjusts the channel spacing between two wavelength-division multiplexing (WDM) channels to be separated. If in particular L_1 and L_2 are different, the interference is between a beam and a delayed version of that beam. With large delay, very fine wavelength discrimination can be performed because the interference pattern can move very rapidly with wavelength. The source beam in our experiments,

Manuscript received July 15, 2004. This work was supported by Defense Advanced Research Projects Agency under the Chip-Scale WDM program through the Army Research Office.

R. Chen and D. A. B. Miller are with Solid State and Photonics Laboratory, Department of Electrical Engineering, Stanford University, Stanford, CA, 94305 USA (e-mail: raychen@stanford.edu).

K. Ma and J. S. Harris, Jr. are with Center for Integrated Systems, Stanford University, Stanford, CA, 94305 USA.

Digital Object Identifier 10.1109/JSTQE.2004.841706

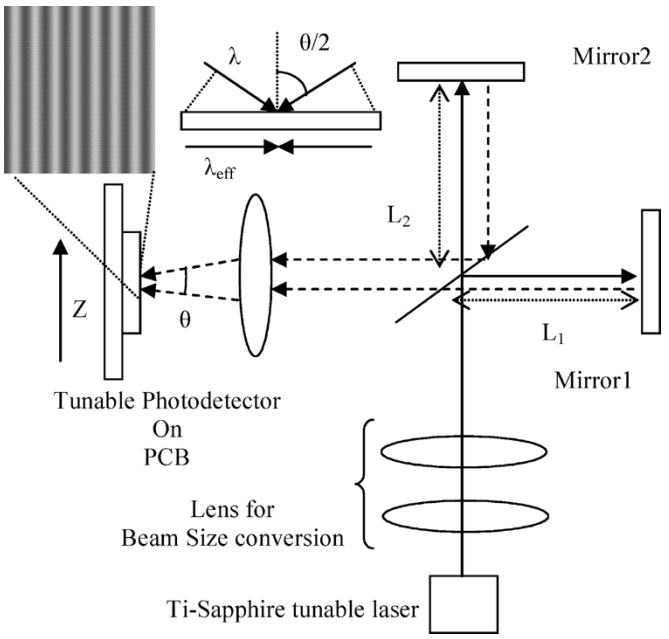

Fig. 1. Michelson interferometer as both standing wave generator and WDM channel spacing controller.

from the Ti-Sapphire tunable laser at the bottom of Fig. 1, is split into two beams by the 50/50 beam splitter. The two beams travel through arms of different lengths, L_1 and L_2, and are reflected back by two mirrors. They then travel almost but, deliberately, not exactly collinearly to get focused so that they overlap on the device, forming an interference pattern. To understand the interference pattern formed on the device, consider for simplicity the interference pattern $I(z,\lambda)$ formed when two uniform beams of equal intensity, one being a delayed version of the other, and both with wavelength $\lambda_0+\Delta\lambda$, are interfered at an angle θ in Fig. 1. If one beam, say the upper one in the figure, travels a longer path by an amount $2|L_2-L_1|=\Delta d$, then the relative phase of the two beams is $\phi(\lambda_0+\Delta\lambda)=2\pi n\Delta d/(\lambda_0+\Delta\lambda)$, where n is the refractive index of the medium in which the beams are propagating (here, air). The interference pattern intensity is given by (1), where $\lambda_{\text{eff}}=(\lambda_0+\Delta\lambda)/\sin(\theta/2)$, the effective projected wavelength on the device, as can be seen in Fig. 1.

$$\begin{aligned} I(z,\lambda) &\propto \left|e^{-j\left(\frac{2\pi n}{\lambda_{\text{eff}}}z\right)}+e^{j\left(\frac{2\pi n}{\lambda_{\text{eff}}}z+\phi(\lambda_0+\Delta\lambda)\right)}\right|^2 \\ &\propto \cos^2\left(\frac{2\pi n}{\lambda_{\text{eff}}}z+\frac{\phi(\lambda_0+\Delta\lambda)}{2}\right) \\ &\approx \frac{1}{2}\left(1+\cos\left(\left(4\pi n\sin\left(\frac{\theta}{2}\right)z+2\pi n\Delta d\right)\right.\right. \\ &\qquad \left.\left.\times\frac{1}{\lambda_0}\left(1-\frac{\Delta\lambda}{\lambda_0}\right)\right)\right) \end{aligned} \tag{1}$$

where the approximation is valid for small $\Delta\lambda$. (For telecommunication applications, the wavelength difference between two WDM channels is insignificant compared to the wavelength λ_0. Ignoring constant terms in (1), the interference pattern intensity for wavelength $\lambda_0+\Delta\lambda$ can be expressed as

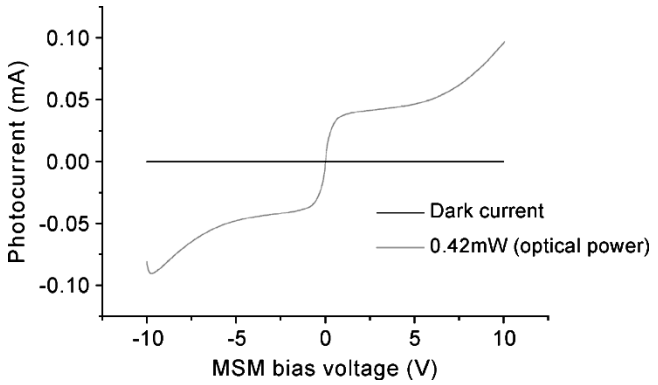

Fig. 2. Photocurrent response of an MSM diode with and without optical power.

in (2), where $k_{\text{int}}=4\pi n\sin(\theta/2)/\lambda_0$, $\beta(\Delta d)=2\pi n\Delta d/\lambda_0$, and $\Phi(\lambda,\Delta d)=2\pi n\Delta d(\lambda-\lambda_0)/\lambda_0^2$

$$\begin{aligned} I(z,\lambda) &\propto \cos\left(\frac{4\pi n\sin\left(\frac{\theta}{2}\right)}{\lambda_0}z+\frac{2\pi n\Delta d}{\lambda_0}-\frac{2\pi n\Delta d\Delta\lambda}{\lambda_0^2}\right) \\ &= \cos\left(k_{\text{int}}z+\beta(\Delta d)-\frac{2\pi n\Delta d(\lambda-\lambda_0)}{\lambda_0^2}\right) \\ &= \cos\left(k_{\text{int}}z+\beta(\Delta d)-\Phi(\lambda,\Delta d)\right). \end{aligned} \tag{2}$$

Note that the interference fringes will move in space as a function of wavelength assuming the path length difference $2|L_2-L_1|=\Delta d$ is fixed. In fact, we can move the pattern by half of the period, π phase shift, by changing the wavelength by a specific value of $\Delta\lambda$, i.e., choosing

$$\Delta\lambda=\left.\frac{\Phi(\lambda,\Delta d)\cdot\lambda_0^2}{2\pi n\Delta d}\right|_{\Phi(\lambda,\Delta d)=\pi}=\frac{\lambda_0^2}{2n\Delta d}. \tag{3}$$

The key idea of the detector's wavelength sensitivity and tunability is that we can set up the detector biasing and finger spacing so that the detector is sensitive to one of the wavelengths λ_0 or $\lambda_0+\Delta\lambda$, but rejects the other one. In order to do that, based on our design algorithm, we would like the interference patterns formed by λ_0 and $\lambda_0+\Delta\lambda$ to be π out of phase with one another as will be explained later in this section. As a result, the required path length difference $\Delta d=2|L_2-L_1|$ in Fig. 1 is inversely proportional to $\Delta\lambda$, the channel spacing between two WDM channels, for fixed relative phase difference between two interference patterns formed by λ_0 and $\lambda_0+\Delta\lambda$. Therefore, varying the path difference between the two beams controls the resolution, with smaller path difference giving larger detectable channel separation. In our optical setup design, the WDM channel spacing has no fundamental limitation, and, we could use this optical setup to resolve very fine dense WDM (DWDM) channels (e.g., less than 50 GHz).

Bipolarity is key feature of the MSM that we use to design the tunable photodetectors. The measured *I-V* curve of the MSM detector is shown in Fig. 2, both with and without continuous-wave (CW) light. As can be seen, the photocurrent has odd symmetry about the zero voltage point. If the MSM photodetector is biased positively, the photocurrent flows from the biasing node to the common ground node. However, if it is biased negatively,

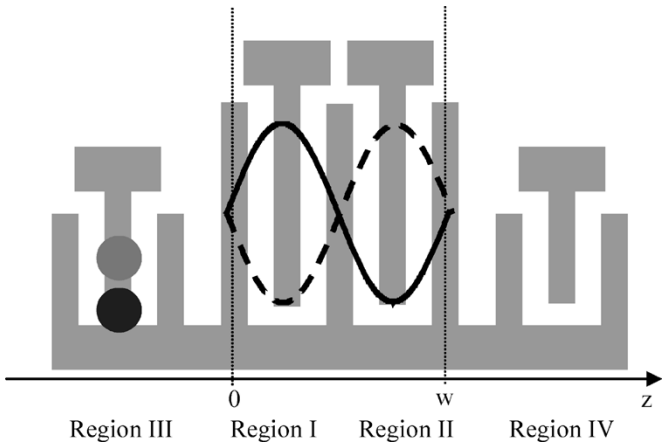

Fig. 3. Tunable MSM device, with interference patterns shown as a solid line and a dashed line, for the two wavelength channels. (Note: each interference pattern has a minimum of zero intensity.) Region III is illuminated by another portion of the total signal beam, and is used to adjust the overall spectral response to achieve a good ON/OFF contrast ratio between the selected and rejected wavelengths. The spacing between interference fringes is controlled by the incident angle of the two interfered beams to fit the width of the center region of the device.

the photocurrent flows from the common ground node to the biasing node. This bipolar nature of MSMs can be used to weight the photocurrent from different parts of the interference pattern illuminated on the device to achieve wavelength sensitive photocurrent output.

The generated interference pattern is oriented to line up with the MSM fingers. We can then bias the two electrodes in the center region of the device in Fig. 3 with opposite polarity to respond to specific interference patterns. The width of the pattern in the center region of the device, w, as shown in Fig. 3, should be the same as the interference pattern period, $\lambda_0/(2n\sin(\theta/2))$ in this design. In practice, the width of a single interference fringe can be controlled by the incident angle, θ in Fig. 1, of the two interfered beams to fit the width of the switching part of the device.

For WDM applications, since the channel spacing $\Delta\lambda$ is much smaller than λ_0, the width of a single fringe formed by $\lambda_0+\Delta\lambda$ and λ_0 is approximately the same. The interference patterns depend on wavelength, primarily through the spatial phase of the pattern and, hence, this device can be a wavelength sensitive photodetector.

To make a detector that can respond to one of λ_0 or $\lambda_0+\Delta\lambda$ and reject the other using the electrode pattern of Fig. 3, we both shine the interfering signal beams on the detector, and also shine another controlled portion of the original signal beam (with no interference) on Region III. This additional beam on Region III is to obtain complete cancellation of the photocurrent from the rejected wavelength, as we will describe later. The electrode in Region III is always positively biased and, hence, always contributes a positive net photocurrent. If we would like to enable the wavelength shown as the solid line interference pattern (formed by λ_0), while disabling the wavelength shown as the dashed line interference pattern (formed by $\lambda_0+\Delta\lambda$), we positively bias the electrode in Region I and negatively bias the electrode in Region II. The positive photocurrent from the $\lambda_0+\Delta\lambda$ portion of the beam on Region III cancels the net negative photocurrent that results from the dashed interference pattern (formed by $\lambda_0+\Delta\lambda$), thereby canceling all the photocurrent for the signal beam at $\lambda_0+\Delta\lambda$. If we would like to enable the dashed interference pattern at $\lambda_0+\Delta\lambda$ while disabling the solid interference pattern at λ_0, we can swap the biasing of Regions I and II (while leaving the biasing of Region III always positive), i.e., positively biasing Region II and negatively biasing Region I with now overall cancellation of the net photocurrent for the signal beam at λ_0. Therefore, by determining the biasing pattern applied on electrodes in Region I and II, we can select one wavelength while deactivating the other. The spectral response of the detector can be derived as follows.

The photocurrent $I_{\rm ph}(\lambda)$ spatially integrated over one period of the interference pattern formed by λ_0, shown as the solid sinusoidal curve in Fig. 3, with the device positively biased in Region I and negatively biased in Region II, can be derived in (4). In (4), the integrated photocurrent $I_{\rm ph}(\lambda)$ is proportional to the wavelength dependent interference pattern $I(z,\lambda)$ weighted by the biasing of the device electrodes. We choose Δd such that $\beta(\Delta d)=-\pi/2$ in $I(z,\lambda)$ in (4). With this choice, the photocurrent spectral response of a single MSM section with half of it positively biased and the other half negatively biased, without considering any effect of the Gaussian shape of the beams, is cosinusoidal in the wavelength domain with center wavelength λ_0. In reality, for MSM devices with equal finger and spacing width, the MSM fingers cover half of the semiconductor surface such that the device will not sense the whole interference pattern. If we take this into consideration in the integral, the coefficient in front of the cosine term in (4) will be reduced from 4 to 2.16, although this will not make any difference to the device design

$$\begin{aligned} I_{\rm ph}(\lambda) &\propto \int_{z=0}^{z=w} I(z,\lambda)|_{\beta(\Delta d)=-\frac{\pi}{2}}\,{\rm V_B}\cdot dz \\ &= \int_{z=0}^{z=\frac{w}{2}} \sin\left(k_{\rm int}z-\Phi(\lambda,\Delta d)\right)dz \\ &\quad - \int_{z=\frac{w}{2}}^{z=w} \sin\left(k_{\rm int}z-\Phi(\lambda,\Delta d)\right)dz \\ &\propto 4\cos\left(\Phi(\lambda,\Delta d)\right) \\ &= 4\cos\left(\frac{2\pi n\Delta d(\lambda-\lambda_0)}{\lambda_0^2}\right). \end{aligned} \tag{4}$$

By adding another wavelength independent term from the signal itself to (4) to nullify the device sensitivity on wavelength $\lambda_0+\lambda_0^2/(2n\Delta d)$, we can get the device spectral response of (5), which has a maximum sensitivity at λ_0 and a null sensitivity at $\lambda_0+\lambda_0^2/(2n\Delta d)$. Therefore, we can discriminate wavelengths between λ_0 and $\lambda_0+\lambda_0^2/(2n\Delta d)$

$$I_{\rm ph}\propto 4\left(\cos\left(\frac{2\pi n\Delta d(\lambda-\lambda_0)}{\lambda_0^2}\right)+1\right). \tag{5}$$

In general, if this device is used to sense ON/OFF modulated signals from two WDM channels, at a given snapshot, the overall photocurrent could be expressed in the following,

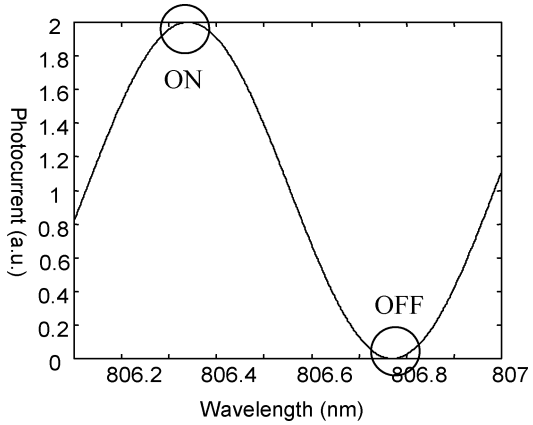

Fig. 4. Simulation of the spectral response of the tunable photodetector enabling 806.34 nm and disabling 806.77 nm. The optical path length difference between the two interfered beams is ∼0.763 mm.

where $A_i = A_{\rm ON}$ or $A_i = A_{\rm OFF}$ and $\lambda_i = \lambda_0$ or $\lambda_i = \lambda_0 + \lambda_0^2/(2n\Delta d)$.

$$I_{ph\_WDM} = \sum_{i=1,2} A_i \left(\cos\left(\frac{2\pi n \Delta d(\lambda_i - \lambda_0)}{\lambda_0^2} \right) + 1 \right). \quad (6)$$

An example device spectral response is simulated in Fig. 4. The simulated device discriminates between its maximum spectral response at 806.34 nm and a null at 806.77 nm, (or *vice versa* depending on finger biasing). The optical path length difference between the two interfered beams is ∼0.763 mm in this simulation, as can be calculated from (3). We have experimentally demonstrated the cosinusoidal spectral response of a single MSM section which is lined up with a single interference pattern period in [11], but we cannot usefully compare the present simulation with experiment for this specific channel spacing because our Ti-Sapphire laser system could not be tuned sufficiently finely to resolve this spectral response curve. In addition, in our actual devices, shown in Fig. 5, we deliberately designed each of the MSM electrodes to have three fingers in each region rather than one to reduce the effects of fabrication variations between the Schottky barriers at each finger, which can lead to slightly different responsivities between positive and negative biasing.

III. Device Structure

The device in Fig. 5 is fabricated on a wafer with a 1 μm thick undoped GaAs epitaxial active layer on a 0.3-μm $Al_{0.85}Ga_{0.15}As$ barrier layer on a semi-insulating GaAs substrate. The fabricated device in Fig. 5 consists of fingers in three regions—left, center and right. The center part, which performs the wavelength switching, comprises two interdigitated sets of three biasing electrodes and one comb-like current summing electrode. All three parts have 1-μm finger width and spacing. The center part covers a 40 × 25 μm area. The left side part covers a 20 × 13 μm area. This is used to adjust the overall spectral response to achieve a good ON/OFF contrast ratio. The right side part of the device, which is a dummy structure device to increase the structural symmetry of the detector for symmetrical ac response, is structurally the same as the left-side part of the device. This part of the device is biased to ground to avoid contributing any noise to the signal photocurrent.

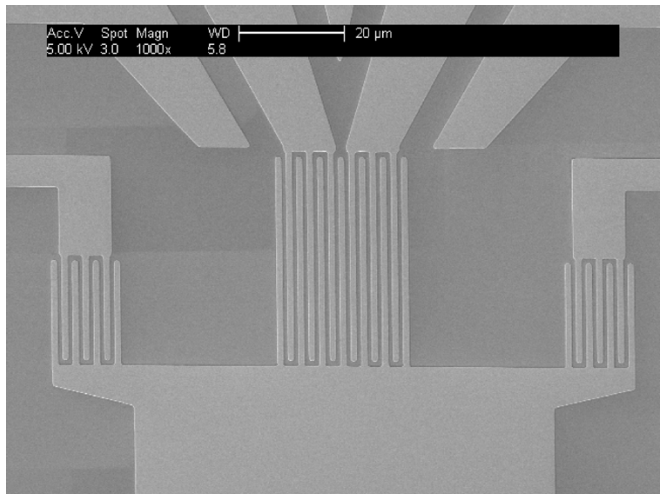

Fig. 5. Scanning electron microscopy photograph of the fabricated tunable photodetector with 1 μm finger spacing and width. The pattern in the center region of the device is used to perform wavelength switching, while the fingers in the left region are used for adjusting the spectral response to achieve a good wavelength-selective contrast ratio. The right region is a dummy structure for symmetry of the device.

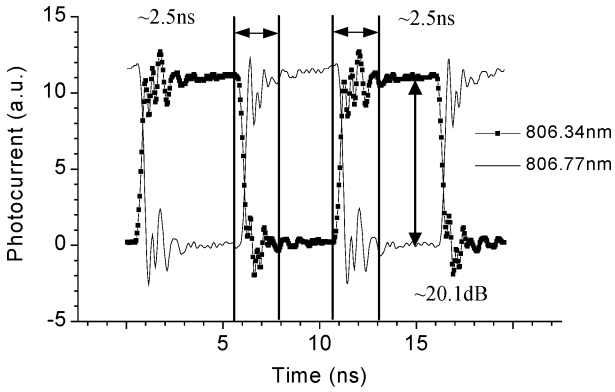

Fig. 6. Photocurrent output of the device as the biasing pattern is changed to select one wavelength or the other. The biasing pattern applied on the device alternates every 5 ns to select between 806.34 and 806.77 nm. The device wavelength switching access time is ∼2.5 ns and the ON/OFF contrast ratio for selecting one wavelength while deactivating the other is ∼20.1 dB.

IV. Results and Discussion

To demonstrate the rapid switching ability of the device in discriminating wavelengths, we used truly differential electrical square waves, toggling every 5 ns between ±1.65 V, to give opposite and alternating bias on the two sets of electrodes in the central region of the device in Fig. 5. The resulting detected photocurrents are shown in Fig. 6 for each of the two chosen wavelengths (806.34 and 806.77 nm). A 2.4-V dc bias voltage is applied on the left region of the device of Fig. 5, and the optical power fraction on this region is adjusted to give the best rejection of the undesired wavelength (this setting is the same for both of the traces in Fig. 6).

The device is directly mounted on a custom designed printed circuit board (PCB) as shown in Fig. 7, without any chip

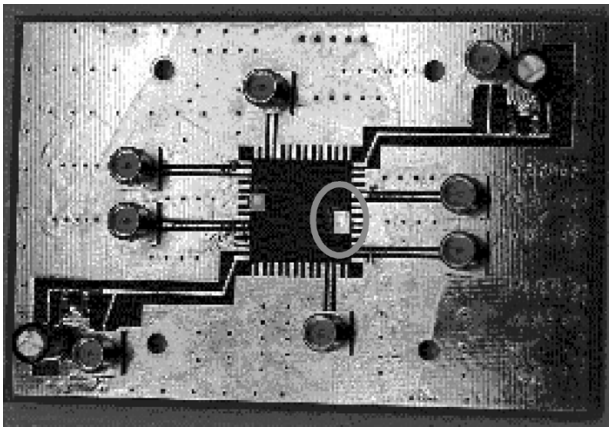

Fig. 7. Tunable photodetector (circled), is shown directly mounted on a custom designed printed circuit board with SMA connectors.

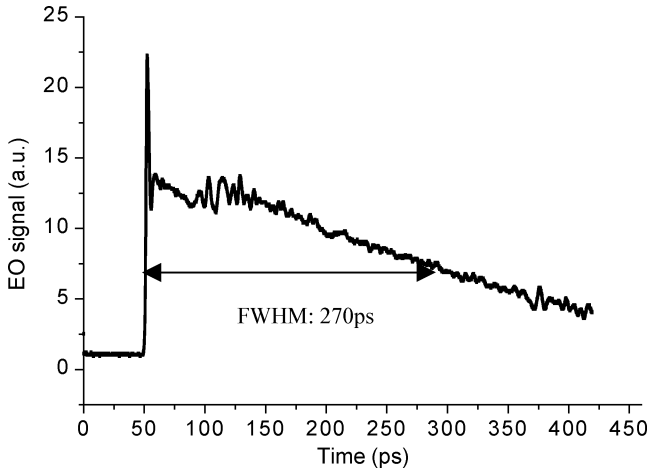

Fig. 8. Intrinsic response of the tunable photodetector measured with a subpicosecond optical input pulse and electrooptic sampling of the output, with 1.65-V bias.

package, to eliminate any ringing from parasitic circuit elements of the package. All of the traces on PCB were designed to be coplanar waveguides, connecting to SMA connectors to reduce the unnecessary electrical coupling and energy reflection. We monitor the photocurrent trace of the device in the time domain through a high speed oscilloscope with 50-Ω input impedance and with an internal 1 GHz low pass filter.

The OFF and ON currents under dc biasing are, respectively, $\sim$ 2.14 and $\sim$ 220 μA under these experimental conditions, and the ON/OFF photocurrent contrast ratio is $\sim$20.1 dB under this specific dc biasing and these interference fringes. (Note that the photocurrent contrast ratio in decibels we calculated here is based on ten times the logarithmic current ratio instead of 20 times the logarithmic current ratio defined in usual electronic decibels definition. This is because this contrast ratio in photocurrent corresponds to $\sim$20.1-dB ON/OFF contrast ratio in optical power.) This ON/OFF contrast ratio under dc biasing is approximately the same as the ON/OFF contrast ratio in Fig. 6 after the ringing has settled down. The device wavelength switching access time is $\sim$2.5 ns, which is limited by the ringing, which we believe is from packaging issues (bonding wires).

We have also measured the optical impulse response of this device, biased under 1.65-V, using a subpicosecond mode-locked laser and electrooptic sampling, as shown in Fig. 8; the full-width at half-maximum (FWHM) of the response under this optical measurement is 270 ps. This FWHM value suggests that the MSM device on this wafer should be able to switch wavelengths in a few hundreds of picoseconds if the electrical parasitic effects can be eliminated. Therefore, a much shorter wavelength switching access time is expected by flip-chip bonding the devices on CMOS electronics to reduce the packaging problems, and this will be the subject of future work.

The channel spacing between the two wavelengths in these measurements is 179 GHz (0.43 nm). This channel spacing is the minimum available from the Ti-Sapphire laser used, and does not represent any apparent limit for the device.

During the experiment, the effect of the Gaussian beam shape is relevant. If the device was not placed at the center of the interference pattern, the switching always favors one side more than the other as we would expect.

V. Conclusion

A novel MSM tunable photodetector for two-wavelength discrimination is proposed, theoretically modeled, and demonstrated. A $\sim$2.5-ns wavelength switching access time and $\sim$20.1-dB ON/OFF contrast ratio between the selected and rejected wavelength of the device have been experimentally demonstrated. This low bias voltage of the device (here $\sim$1.65 V) makes it compatible with standard CMOS control electronics to construct a chip-scale rapidly tunable photoreceiver. We expect this kind of tunable photodetector discussed here could be used as part of a future dynamic wavelength allocation optical network, with switching much shorter than time scales corresponding to packet lengths, or possibly even bit periods. It could also enable rapidly tunable optical receivers for optical code-division multiple-access networks.

Acknowledgment

The authors would like to thank R. Urata, Y. W. Lee, H. Chin, and M. Weimer for stimulating discussions.

References

[1] I. M. White, M. S. Rogge, K. Shrikhande, and L. G. Kazovsky, "A summary of the HORNET project: A next-generation metropolitan area network," *IEEE J. Select. Areas Commun.*, vol. 21, no. 9, pp. 1478–1494, Nov. 2003.

[2] Y. L. Hsueh, M. S. Rogge, W. T. Shaw, L. G. Kazovsky, and S. Yamamoto, "SUCCESS-DWA: A highly scalable and cost-effective optical access network," *IEEE Commun. Mag.*, vol. 42, no. 8, pp. S24–S30, Aug. 2004.

[3] K. W. Cheung, "Acoustooptic tunable filters in narrowband WDM networks: System issues and network applications," *IEEE J. Select. Areas Commun.*, vol. 8, no. 6, pp. 1015–1025, Aug. 1990.

[4] A. Iocco, H. G. Limberger, R. P. Salathe, L. A. Everall, K. E. Chisholm, J. A. R. Williams, and I. Bennion, "Bragg grating fast tunable filter for wavelength division multiplexing," *IEEE J. Lightw. Technol.*, vol. 17, no. 7, pp. 1217–1221, July 1999.

[5] T. Amano, F. Koyama, T. Hino, M. Arai, and A. Mastutani, "Design and fabrication of GaAs-GaAlAs micromachined tunable filter with thermal strain control," *IEEE J. Lightw. Technol.*, vol. 21, no. 3, pp. 596–601, Mar. 2003.

[6] S. Suzuki *et al.*, "Integrated multichannel optical wavelength selective switches incorporating an arrayed-waveguide grateing multiplexer and thermooptic switches," *J. Lightw. Technol.*, vol. 16, no. 4, pp. 650–655, Apr. 1998.

[7] K. Lai and J. C. Campbell, "Design of a tunable GaAs/AlGaAs multiple-quantum-well resonant-cavity photodetector," *IEEE J. Quantum Electron.*, vol. 30, no. 1, pp. 108–114, Jan. 1994.
[8] J. P. Weber *et al.*, "An integratable polarization-independent tunable filter for WDM systems: The multigrating filter," *J. Lightw. Technol.*, vol. 14, no. 12, pp. 2719–2735, Dec. 1996.
[9] E. L. Wooten *et al.*, "Rapidly tunable narrowband wavelength filter using $LiNbO_3$ unbalanced Mach-Zehnder interferometers," *J. Lightwave Technol.*, vol. 14, no. 11, pp. 2530–2536, Nov. 1996.
[10] D. A. B. Miller, "Lasers tuners and wavelength-selective detectors based on absorbers in standing waves," *IEEE J. Quantum Electron.*, vol. 30, no. 3, pp. 732–749, Mar. 1994.
[11] R. Chen, H. Chin, and D. A. B. Miller, "Novel electrically tunable MSM photodetector for resolving WDM channels," in *Proc. IEEE Lasers Electro-Optics Soc.*, vol. 2, 2003, Paper WCC5, pp. 724–725.

Ray Chen (S'01) received the B.Sc. degree in electronics engineering from National Chiao Tung University, Hsin-Chu, Taiwan, R.O.C. in 1997, and the M.S. degree in electrical engineering in 2001, from Stanford University, Stanford, CA, where he is currently working toward the Ph.D. degree under Prof. D. A. B. Miller. His doctoral research focuses on CMOS controlled rapidly tunable photodetectors for access network and telecommunication applications.

From 1997 to 1999, he served in the Chinese Army as a Communication Technical Officer. During the summer of 2000, he interned at IBM Microelectronics, Essex Junction, VT, where he was working on IC testing methodology for ASICs.

David A. B. Miller (M'84–SM'89–F'95) received the B.Sc. degree from St. Andrews University, Fife, Scotland, U.K., and the Ph.D. degree from Heriot-Watt University, Edinburgh, Scotland, in 1979.

He was with Bell Laboratories, Holmdel, NJ, from 1981 to 1996, as a Department Head from 1987, latterly of the Advanced Photonics Research Department. He is currently the W. M. Keck Professor of Electrical Engineering at Stanford University, Stanford, CA, and the Director of the Ginzton and Solid State and Photonics Laboratories, Stanford, CA. He has published more than 200 scientific papers, and holds over 55 patents. His research interests include quantum-well optoelectronic and nanophotonic physics and devices, and fundamental and applications of optics in information, sensing, switching, and processing.

Dr. Miller has served as a Board Member for both the Optical Society of America (OSA) and IEEE Lasers and Electro-Optics Society (LEOS), and in various other society and conference committees. He was President of the IEEE Lasers and Electro-Optics Society in 1995. He was awarded the Adolph Lomb Medal and the R. W. Wood Prize from the OSA, the International Prize in Optics from the International Commission for Optics, and the IEEE Third Millennium Medal. He is a Fellow of the Royal Societies of London and Edinburgh, OSA, and the American Physical Society, and holds honorary degree from the Vrije Universiteit Brussel and Heriot-Watt University.

Kai Ma (S'03) received the B.S. and M.S. degrees in materials science and engineering from Tsinghua University, Beijing, China, in 1993 and 1996, respectively, and the M.S. degree in electrical engineering in 2003, from Stanford University, Stanford, CA, where she is currently working toward the Ph.D. degree in materials science and engineering.

She is a Research Assistant with Solid State and Photonics Laboratory, Stanford University. Her current research has been focused on the study of MBE-grown III-V materials and the novel integration of GaAs photonic devices with Si CMOS circuits.

James S. Harris, Jr. (S'65–M'69–SM'78–F'88) received the B.S., M.S., and Ph.D. degrees in electrical engineering from Stanford University, Stanford, CA, in 1964, 1965, and 1969, respectively.

In 1969, he joined the Rockwell International Science Center, Thousand Oaks, CA, where he was one of the key contributors in developing their preeminent position in GaAs device technology. In 1982, he joined the Solid State Electronics Laboratory, Stanford University, as Professor of Electrical Engineering. He served as Director of the Solid State Electronics Laboratory (1984–1998) and the Joint Services Electronics Program (1985–1999), Stanford University. He is currently the James and Ellenor Chesebrough Professor of Engineering at Stanford University. He has supervised over 65 Ph.D. students, has over 650 publications, and 14 issued U.S. patents. His current research interests are in the physics and application of ultrasmall structures and novel materials to new high-speed and spin-based electronic and optoelectronic devices and systems.

Dr. Harris is a Fellow of the American Physical Society. He received the 2000 IEEE Morris N. Liebmann Memorial Award, the 2000 International Compound Semiconductor Conference Walker Medal, an IEEE Third Millennium Medal, and an Alexander von Humboldt Senior Research Prize in 1998 for his contributions to GaAs devices and technology.